PAPER

Check for updates

Selective growth inhibition of cancer cells with doxorubicin-loaded CB[7]-modified iron-oxide nanoparticles†

F. Benyettou,[a] H. Fahs,[a] R. Elkharrag,[a] R. A. Bilbeisi,[a] B. Asma,[a] R. Rezgui,[a] L. Motte, [b] M. Magzoub,[a] J. Brandel,[c] J.-C. Olsen,[d] F. Piano,[ae] K. C. Gunsalus,[ae] C. Platas-Iglesias[f] and A. Trabolsi [*a]

Cucurbit[7]uril-modified iron-oxide nanoparticles (CB[7]NPs) were loaded with doxorubicin hydrochloride (Dox) and tested as a drug delivery system. Dox was found to interact with the carbonyl-rich rims of the CB[7] macrocycles adsorbed on the surface of the nanoparticles. The Dox-loaded nanoparticles (Dox@CB[7]NPs) were stable at room temperature and physiological pH and released their Dox cargo under acidic conditions, in the presence of glutathione, or with heating. Dox@CB[7]NPs reduced the viability of HeLa and three other cancer-derived cell lines *in vitro* at lower IC_{50} than free Dox. They were also nontoxic to *C. elegans*. The sensitivity of HeLa cells to Dox@CB[7]NPs was enhanced when the temperature was elevated by application of an alternating magnetic field. Thus, Dox@CB[7]NPs show promise as agents for the intracellular delivery of Dox to cancer cells, for the selective and controlled release of the drug, and, more generally, as a possible means of combining chemotherapeutic and hyperthermic treatment modalities.

Introduction

Cytotoxic drugs inhibit the growth of primary and metastatic tumors.[1,2] However, traditional drug delivery methods require high dosing, are non-selective and cause serious side-effects.[3] With advances in material design and an ever-increasing understanding of the physiological differences between normal and diseased tissue, researchers are developing target-specific nanocarrier systems that deliver drugs intracellularly for selective and controlled release.[4,5] Selective cell targeting and intracellular delivery/release increase the effectiveness of anticancer drugs by lowering required dosages and sparing normal tissue.[6]

Iron oxide nanoparticles (NPs) are versatile drug carriers that have unique features.[7] Not only can they deliver drugs to

[a]*New York University Abu Dhabi, Abu Dhabi, United Arab Emirates. E-mail: ali. trabolsi@nyu.edu*

[b]*Université Paris 13, Sorbonne Paris Cité, Laboratoire CSPBAT, CNRS, UMR 7244, F-93017, Bobigny, France*

[c]*Equipe Reconnaissance et Procédés de Séparation Moléculaire, Université de Strasbourg, IPHC, 67087 Strasbourg, France*

[d]*Department of Chemistry, University of Rochester, RC Box 270216, Rochester, NY 14607-0216, USA*

[e]*Center for Genomics and Systems Biology, Department of Biology, New York University, New York, NY 10003, USA*

[f]*Departamento de Química Fundamental, Universidade da Coruña, Campus da Zapateira, Rúa da Fraga 10, 15008 A Coruña, Spain*

† Electronic supplementary information (ESI) available. See DOI: 10.1039/c7ra02693e

diseased tissue,[8] but they can also function as MRI contrast agents[9] and as mediators of hyperthermia treatment.[10] The design and synthesis of NPs modified with the water-soluble macrocycle curbit[7]uril (CB[7]) have been described previously by our group as well as by Yang *et al.*[11,12] We demonstrated that these modified NPs (CB[7]NPs) adsorb and intracellularly deliver the fluorophore Nile red and that they exhibit transverse relaxivity (R_2) suitable for MRI contrast enhancement ($R_2 = 113$ and 172 s^{-1} mM^{-1} for CB[7]NPs and dye-loaded CB[7]NPs, respectively).[11]

Since CB[7] forms non-covalent but relatively strong complexes with small organic molecules that contain the ammonium group,[13,14] we anticipated that CB[7]NPs would also adsorb the potent anticancer drug doxorubicin hydrochloride (Dox). Here we show that the ammonium group of Dox binds to the carbonyl-rich rim of surface-attached CB[7] and that the resulting drug-loaded particles (Dox@CB[7]NPs) are stable at room temperature and physiological pH but release Dox (Fig. 1) when stimulated by low pH, glutathione (GSH), or heat. Hydronium ions hydrogen-bond to the carbonyls of CB[7] at low pH [15] and thereby interfere with CB[7]-Dox complexation; GSH,[16,17] a small ammonium-containing tripeptide, disrupts CB [7]-Dox complexation in a similar way and heat, in general, destabilizes host–guest complexes.[18]

The first two release stimuli, acidic pH and GSH, are, to varying degrees, specific to cancer. The extracellular pH of cancer tissue generally ranges from 5.8 to 7.0, whereas the pH of normal tissue and the bloodstream is about 7.4.[19,20] Cancer
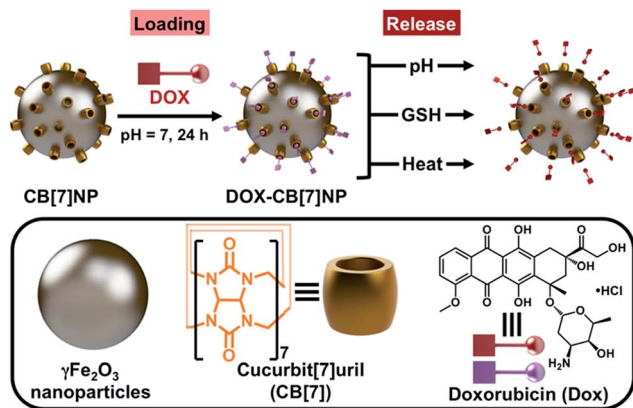
Fig. 1 Schematic representation (top) of the loading and release of Dox from a CB[7]NP. Dox is released at low pH, in the presence of GSH, or with heating. Surface-adsorbed Dox (purple symbol with square) was found to fluoresce less intensely than free Dox (red symbol with square).

tissue tends to be more acidic because its cells usually contain greater numbers of lysosomes and endosomes.[21] With regard to GSH, several intracellular compartments such as the cytosol, mitochondria and cell nuclei contain concentrations of the peptide (2–10 mM) that are 100–1000 times higher than those in extracellular fluids and the bloodstream (2–20 μM),[22] and cytosolic GSH concentrations in certain types of tumor cells have been found to be up to seven times higher than those in normal cells.[23] Because of these differences, GSH is well-recognized as a convenient stimulus for nanocarrier destabilization and intracellular drug release.[24–27]

The third stimulus, heat, can be induced by application of an alternating magnetic field (AMF), which causes iron-oxide nanoparticles to vibrate and to raise the temperature of surrounding tissue.[28] AMF-induced heating has been used previously to release drugs that have been bound directly to nanoparticles[29] or that have been embedded within polymeric matrices coating particles.[30,31] Hyperthermia can also act as a direct anticancer treatment.[32,33] For a given NP size, temperature is determined by heating time.[34] With short heating times and relatively low temperatures (∼40 °C), cancer cells are weakened.[35] With longer times and higher temperatures (>42 °C), cancer cells are destroyed by a process known as thermal ablation.[36] Furthermore, hyperthermia can act synergistically with nanoparticle-delivered chemotherapy.[37]

In the rapidly developing field of bio-nanotechnology, reliable methods for determining the safety and effectiveness of nanomaterials are required. In that regard, the nematode Caenorhabditis elegans (C. elegans) has emerged as an attractive animal model for drug screening and delivery as a result of its simple body plan, fully characterized cell lineage and genome sequence, and ease of cultivation in the laboratory.[38,39] Moreover, biological mechanisms are highly conserved between C. elegans and vertebrates, and evidence is accumulating that in vivo results from C. elegans can be predictive of outcomes in higher organisms.[40,41] These benefits together with its simplicity and cost effectiveness make C. elegans a powerful model for research.[42–44]

Results and discussion

We began the present study by simulating with DFT calculations the mode of interaction between Dox and CB[7]. Subsequent ^{1}H NMR and FTIR spectroscopy, as well as thermogravimetric analysis, provided both qualitative and quantitative support for the binding model deduced from computations. We found that release of Dox is pH- and GSH-sensitive, which allows for intracellular release of Dox both in the cytosol and within the acidic microenvironments of late endosomes and lysosomes. Dox release is also temperature dependent, and gradual release can be triggered by magnetically heating a solution of Dox@CB[7]NPs. Finally, we found that the drug-loaded particles were more effective than free Dox at decreasing the viability of cervical epithelial cancer cells (HeLa), breast cancer cells (MCF-7), ovarian cancer cells (A2780), and doxorubicin-resistant ovarian cancer cells (A2780/AD). Furthermore, the cytotoxic effects of the nanoparticles on HeLa cells were drastically enhanced by hyperthermia treatment. Remarkably, while Dox is not selective to cancer cells, Dox@CB[7]NPs showed minimal toxicity when incubated with a non-cancerous cell line derived from human embryonic kidney cells (HEK293) as a result of the limited cell uptake of the NPs indicated by magnetic measurements. Treatment of C. elegans with either CB[7]NPs or Dox@CB[7]NPs at comparable concentrations for up to 7 days resulted in no observable decrease in viability, growth, or reproduction.

Macrocycles and IONPs are common components of DDSs; however, examples of systems that incorporate macrocycle-modified iron oxide NPs in which the macrocycle is directly attached to the surface of the nanoparticles are still rare. The direct conjugation of calixarenes and cyclodextrins to the surface of IONPs for drug delivery applications has been reported by Chin and co-workers[45] and Yallapu and co-workers,[46] respectively. Our group was the first to report the synthesis of IONPs with cucurbituril directly attached. A major advantage of this modification is the stabilization that the macrocycle confers, specifically, its minimization of particle aggregation at physiological pH.[11] There are other systems in which cucurbituril and IONPs have been combined; however, in these, the cucurbituril is used not as a drug host but as a gatekeeper that indirectly prevents drug release.[47,48] Our strategy takes advantage of CB[7]'s ability to directly bind Dox molecules via weak non-covalent interactions and to controllably release the drug upon disruption of those supramolecular interactions. Also, in our system, the nanoparticles are utilized as both vehicles for the delivery of Dox and as heat mediators that allow for on-demand release of the drug. Finally, the magnetism of the particles themselves has the potential to allow for in vivo localization.

Dox–CB[7] interaction

The interaction between Dox and free CB[7] was first evaluated computationally using DFT calculations at the b3lyp/6-31G(d,p) level (Fig. 2A and S25†). According to our calculations and in a 1 : 1 stoichiometry, Dox sits on one portal of CB[7] with the
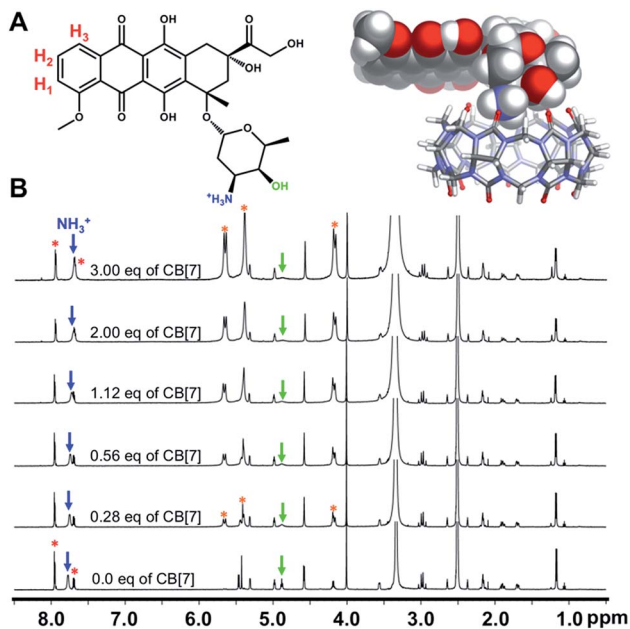
Fig. 2 (A) ChemDraw representation of Dox (top, left) with the aryl protons labeled in red, the ammonium group in blue, and the hydroxyl group in green, and DFT-optimized structure (top, right) illustrating the mode of interaction between Dox and CB[7]; (B) ^{1}H NMR spectra (600 MHz, 298 K) that illustrate changes in the chemical shifts of Dox signals that result from the titration of a solution of Dox (0.86 mM) in d_6-DMSO with increasing amounts of CB[7]. The aryl, ammonium, and hydroxyl proton signals are labeled with red dots, blue arrows, and green arrows, respectively. The CB[7] peaks are labeled with orange dots.

oxygen atoms of the latter acting as hydrogen bond acceptors to the –NH$_3^+$ and –OH groups of the sugar of Dox (Fig. 2A).

The interaction of Dox with free CB[7] was also investigated in solution by titration (Fig. 2B and S26†). A DMSO solution of Dox was titrated with increasing amounts of CB[7] and monitored by ^{1}H NMR spectroscopy. Fig. 2B shows the corresponding spectra, which reveal shifts of several Dox resonances including a noticeable upfield movement (7.75 to 7.69 ppm) of the signal that corresponds to the ammonium protons. Also, there is a significant broadening of the signal at 4.9 ppm, a change that reflects a hydrogen bonding interaction between the hydroxyl proton of the Dox sugar moiety and a carbonyl oxygen of CB[7]. These spectral changes are consistent with the DFT-based binding model.

However, determination of a binding constant for the Dox-CB[7] complex from the NMR data was not possible because of the relatively weak spectral changes and poor solubility of CB[7]. Accurate determination by isothermal titration calorimetry (ITC) was thwarted, under our experimental conditions, by the minimal heat of reaction associated with binding. We inferred, nevertheless, that a binding interaction similar to the one predicted theoretically would occur between Dox and CB[7] macrocycles adsorbed on the surface of NPs and would facilitate drug delivery.

Dox loading and stability of Dox-loaded CB[7]NPs

Spherical CB[7]NPs[11] of 8–10 nm crystalline diameter and an average of 28 CB[7]s per NP were mixed with Dox in a 1 : 1.1

molar ratio in water at pH 7 and room temperature for 24 hours. The resulting brown precipitate was dialyzed for two days and analyzed by FTIR spectroscopy (Fig. S1†). The resulting IR spectrum differs from the sum of the spectra of the two separate components—for example, absorption bands corresponding to CB[7]NPs are shifted and new peaks appear between 1600 and 900 cm^{-1}—therefore confirming an interaction between Dox and the CB[7]NPs. TGA measurements (Fig. S4†) indicated an average ratio of Dox to CB[7] of 1 : 1.

DLS measurements (Fig. S5†) revealed that addition of Dox to CB[7]NPs changes the overall charge on the surface of the particles. The isoelectric point shifted from pH 8.9 for CB[7]NPs to pH 3.7 for Dox@CB[7]NPs. Moreover, at pH 7.4, the ζ-potential of the particles changed from +35 mV to −20 mV. Importantly, although the sign of the potential changed, its magnitude remained sufficient to minimize aggregation and maintain particle stability at physiological pH.

Solution Dox release studies

After establishing the presence of Dox on the surface of Dox@CB[7]NPs and fully characterizing the loaded nanoparticles in solution, we monitored the three release mechanisms by fluorescence spectroscopy. Free Dox can be observed by exciting samples with 488 nm wavelength light, which the free drug absorbs maximally. At pH 7.4, room temperature and in the absence of GSH, Dox fluorescence is quenched by the drug's close proximity to the surface of the nanoparticles (Fig. S8†).[49] This allowed us to measure the amount of Dox released as a function of time and temperature in response to low pH, GSH, or heat.

Fig. 3A indicates the rate of release that occurred in phosphate buffered saline (PBS, 10 mM) under several conditions. A minimal amount of Dox (10% over 4 days) was released at pH 7.4 and room temperature, as indicated by the small increase in emission intensity. This result demonstrates that Dox@CB[7]NPs are relatively stable at physiological pH and room temperature. After acidification of the solution to pH 5.4, 95% of the drug was released into solution over two days, a result that can be attributed to the competitive binding of hydronium ions (H$_3$O$^+$) to the carbonyls of CB[7].[15] A gradual release process such as this could be used for therapeutic purposes if the
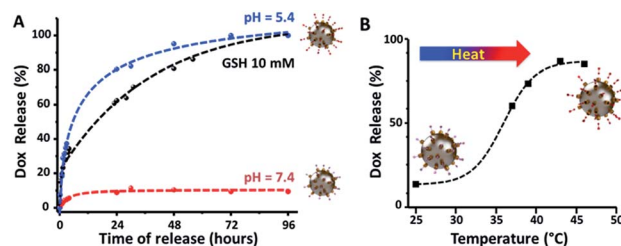

Fig. 3 (A) *In vitro* Dox release profiles of Dox@CB[7]NPs in a PBS solution (10 mM) at pH 7.4 without (red curve) and with (black curve) 10 mM GSH, and at pH 5.4 without GSH (blue curve). (B) *In vitro* Dox release profile of Dox@CB[7]NPs in aqueous solution at pH 7.4, as a function of temperature.

particles were localized at a desired site for the duration of release. Exposure of the Dox@CB[7]NPs to a 10 mM solution of GSH in PBS (10 mM) also caused Dox release, likely as the result of displacement of the drug from the CB[7] cavity by the peptide. Additional evidence for an interaction between GSH and CB[7] was provided by results of ^{1}H NMR titration and ITC titrations of a solution of GSH with free CB[7] (Fig. S27–S30†). The gradual shifting of the GSH proton signals that occurred in the NMR titration with increased CB[7] concentration is consistent with an interaction between the peptide and the macrocycle in solution. Furthermore, the ITC titrations allowed us to determine a stability constant of 3.16 ± 0.05 ($\log K$) for the formation of the 1 : 1 inclusion complex CB[7]⊃GSH in water. This value is similar in magnitude to the stability constant that characterizes the known CB[6]⊃GSH complex.[50]

Additionally, the fluorescence of Dox@CB[7]NPs was measured in fetal bovine serum (FBS) over time (Fig. S9†). Negligible release of the drug was observed after four days at pH 7.4. The pH of the sample was then lowered to 5.4 to mimic conditions within lysosomes, and the change triggered an immediate release of the drug, with complete release achieved after three more days. Together, these results confirm the stability of Dox@CB[7]NPs and that insignificant drug leakage occurs under conditions that mimic an extracellular physiological environment. They also suggest that Dox-CB[7] complexes are more stable on the surface of the nanoparticles than when they are free in solution.

Magnetic and heating properties in solution

After assessing chemically-induced release mechanisms, and in view of potential hyperthermia applications, we subjected Dox@CB[7]NPs to conventional heating. As illustrated in Fig. 3B, when a solution of Dox@CB[7]NPs was heated with a thermomixer, ~90% release of Dox was achieved as the temperature reached 45 °C, demonstrating that heat efficiently disrupts Dox-CB[7] complexation.

Before subjecting the particles to an alternating magnetic field (AMF) to assess their magnetically-induced heating properties, we first measured the magnetic properties of the nanoparticles using a vibrating sample magnetometer (VSM). The magnetization curves for both CB[7]NPs and Dox@CB[7]NPs are characteristic of superparamagnetic nanoparticles[51] and are consistent with maghemite nanoparticles of 8–10 nm diameter[52] (Fig. S7†). Dox@CB[7]NPs exhibited a significantly greater M_{sat} than CB[7]NPs (45.1 emu g^{-1} *versus* 18.8 emu g^{-1}, respectively), which can be explained by the increased aggregation of Dox@CB[7]NPs and the fact that cooperative magnetic behavior is induced when individual particles aggregate.[53] At pH 7, Dox@CB[7]NPs also have a much larger average hydrodynamic diameter than CB[7]NPs (76 nm *versus* 23 nm), due to their greater inter-particle hydrophobic attractions as a result of being coated with hydrophobic Dox molecules,[54] as do CB[7]NPs loaded with Nile red or viologen.[11,55] However, the aggregation of Dox@CB[7]NPs is much less pronounced than that observed for bare NPs (whose hydrodynamic diameter is 5590 nm at pH 7) and not likely to preclude *in vivo* applications.[56] Furthermore,

the superparamagnetism and M_{sat} values of the drug-loaded particles make them ideal agents for magnetic fluid hyperthermia treatments and on-demand, magnetically controlled drug release.[37]

Solutions containing either bare NPs, CB[7]NPs or Dox@CB[7]NPs, each at 0.2 M iron concentration and room temperature, were placed inside a water-cooled copper coil that produced an AMF of 464 kHz frequency and 26.8 kA m^{-1} amplitude. Sample temperature was monitored and found to increase to a maximum of 44 °C, 57 °C or 66 °C when containing NPs, CB[7]NPs, or Dox@CB[7]NPs, respectively (Fig. 4A). The samples that contained particles of larger hydrodynamic radii rose to higher temperatures, consistent with previously reported results.[34] Sample temperature decreased to room temperature in all cases when the oscillating magnetic field was removed.

Dox@CB[7]NPs lost 70% of their drug cargo after 10 minutes of heating under AMF (of 464 kHz frequency and 26.8 kA m^{-1} amplitude when the temperature had reached 43 °C) and 100% after 30 minutes of heating (when the temperature had reached 66 °C), as indicated by Dox fluorescence intensity measurements (Fig. 4B). These results demonstrate the potential of Dox@CB[7]NPs to act as bifunctional agents with chemo- and thermo-therapeutic modes of action.

In vitro biological studies

***In vitro* internalization studies.** We examined the internalization of Dox@CB[7]NPs into HeLa cells incubated for two hours at 37 °C with either Dox@CB[7]NPs or free Dox at equivalent doses of the drug (Fig. 5).

The normalized intracellular fluorescence intensity detected in samples incubated with Dox@CB[7]NPs was approximately two and a half times greater than that detected in samples incubated with free Dox, establishing the effectiveness of CB[7]NPs as a Dox delivery vehicle in this cell type.

To determine the nature of the active entry mechanisms of Dox@CB[7]NPs and the relative contribution of these mechanisms to cellular uptake, we measured fluorescence intensity inside HeLa cells in the presence of chemical inhibitors of the various endocytic pathways (Fig. S15†). We found that macropinocytosis and caveolin-dependent endocytosis are the
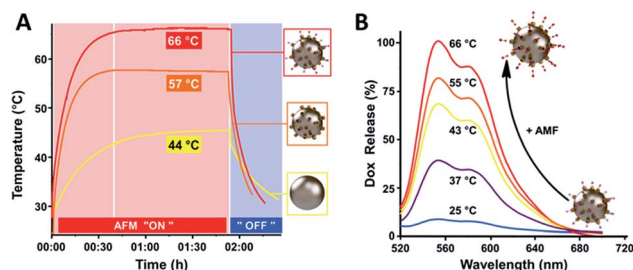

Fig. 4 (A) Temperature response curves for solutions (pH = 7.4, [Fe] = 0.2 M) of bare NPs (yellow), CB[7]NPs (orange) and Dox@CB[7]NPs (red) upon application and removal of a 464 kHz AMF; (B) Dox fluorescence emission spectra (λ_{ex} = 488 nm) of a solution (pH = 7, [Fe] = 0.05 M) of Dox@CB[7]NPs at various temperatures. Dox fluorescence intensity gradually increased as the temperature of the solution rose.
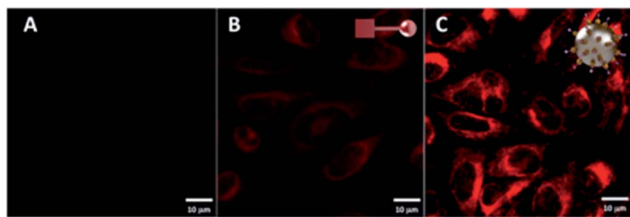
Fig. 5 Confocal laser scanning images of HeLa cells after (A) no treatment, and (B, C) two-hour incubation with [Dox] = 10 μM, using (B) free Dox or (C) Dox@CB[7]NPs. Red fluorescence at λ_{ex} = 488 nm indicates Dox accumulation.

primary uptake mechanisms. When lysosome acidification was inhibited with ammonium chloride, Dox release was significantly inhibited, indicating that acidification is a main trigger for drug release. However, some fluorescence was still apparent in the cytoplasm, which we interpret to reflect the high concentration of GSH within these cancer cells.[24]

The number of CB[7]NPs absorbed by cultured HeLa or HEK293 cells was determined by monitoring the non-linearity of sample magnetization with a MIAtek reader.[57] The MIAtek signal is proportional to the mass of magnetic particles present and allows for the detection of nanograms of superparamagnetic materials.[58] Biological samples exhibit only diamagnetism, a linear magnetic behavior that does not affect the measurement of nonlinear magnetization.[59] We first obtained a calibration curve by measuring the magnetization of samples containing several concentrations of CB[7]NPs (Fig. S15†); we then estimated the average number of CB[7]NPs per cell by dividing the total amount of iron measured by the number of cells present (Fig. S16†). Following incubation times ranging from two to 48 hours, the amount of iron within HeLa cells increased with time and reached a plateau after 24 hours (Fig. S16†). For an extracellular iron concentration of 300 μM, the mean number of CB[7]NPs detected per cell was significantly higher in HeLa (2.3×10^6 NPs) than in HEK293 cells (10^4 NPs), indicating that the malignant cells internalize about 230 times more particles.

In vitro toxicity assessment. We incubated HeLa cells as well as MCF-7, A2780, Dox-resistant A2780, and HEK293 cells for 48 hours with either Dox@CB[7]NPs or free Dox at the same concentration. Cytotoxicity was measured to determine IC_{50} values of Dox@CB[7]NPs and Dox in each cell line (Table 1 and Fig. S17†). Dox@CB[7]NPs showed significantly higher cytotoxicity than free Dox on all four cancer cell lines; thus, when Dox was coupled to the nanoparticles, a lower dose of Dox was required to achieve the same effect.

Notably, the enhanced sensitivity of A2780/AD cells to Dox@CB[7]NPs (Fig. S17D†) demonstrated that, in contrast to free Dox, nanoparticles are capable of overcoming drug resistance in this cell line, as the IC_{50} of Dox@CB[7]NPs in A2780/AD cells (0.6 μM) was comparable to that in the (non-resistant) A2780 parent cell line (0.8 μM). This effect is likely due to the different mode of cell penetration and consequent higher internalization yields afforded by nanoparticle-mediated drug delivery. Similar results and conclusions have been reported for other drug delivery systems.[60,61]

Table 1 Cytotoxicities (IC_{50}) of Dox and Dox@CB[7]NPs against selected human cell lines after 48 hours of treatment[a]

	IC_{50} (μM)	
	Dox	Dox@CB[7]NPs
HeLa	2.4	0.5
MCF-7	1.3	0.6
A2780	20.1	0.8
A2780/AD	>100	0.6
HEK293	0.9	≫100

[a] HeLa = human cervical epithelial carcinoma; MCF-7 = human breast adenocarcinoma; A2780 = human ovarian carcinoma; A2780/AD = human ovarian carcinoma (multi-drug resistant); HEK293 = human embryonic kidney-derived cell line.

In contrast to the four cancer cell lines tested, while the non-cancer-derived cell line HEK293 showed high sensitivity to free Dox under the same conditions (0.9 μM), minimal cytotoxicity was observed for Dox-loaded nanoparticles (IC_{50} was not reached even at the highest concentrations of Dox@CB[7]NPs tested) (Fig. S18†). These results are consistent with both our observations of their lower uptake capacity and previously documented differences in cytoplasmic conditions (including lower GSH concentration and higher pH) in comparison with HeLa cells.[62]

In vitro hyperthermia. To evaluate the hyperthermic effects of the nanoparticles, HeLa cells were incubated for two hours at 37 °C in the presence or absence of Dox@CB[7]NPs or free Dox and then subjected to an alternating magnetic field for 30 minutes. A probe placed in the cell medium recorded the temperature (Fig. S20†). The temperature of cells incubated with Dox@CB[7]NPs rose to 44 °C, whereas the temperature of untreated cells rose to only 33 °C (the AMF instrument does not maintain cells at 37 °C during AMF sessions; however, no cytotoxic effects were observed in cells that had been treated with AMF exposure alone for 2 hours). Optical microscopy (Fig. S21†) revealed the morphology of the cells after treatment. We noticed morphological changes only in Dox@CB[7]NP-treated cells, most of which appeared apoptotic and displayed loss of membrane integrity. HeLa cells treated in the same manner with free Dox showed normal morphology after treatment, as did cells that were heated without exposure to Dox or nanoparticles.

Finally, cell viability tests were performed in order to evaluate the combined effects of hyperthermia and chemotherapy. HeLa cells were incubated for two hours at 37 °C with no additives, free Dox, CB[7]NPs or Dox@CB[7]NPs; selected samples from each of these four treatment groups were then subjected to AMF (464 kHz) for one hour (Fig. 6). We observed minimal reductions in viability in the samples that had been incubated with no additives, Dox, or CB[7]NPs, whether subjected to AMF or not. The lack of significant cytotoxicity in the cells incubated with Dox is consistent with the short incubation time (2 hours). The lack of toxicity in the cells treated with CB[7]NPs alone is due to lower heating properties under our conditions (Fig. 4). The viability of cells treated with Dox@CB[7]NPs
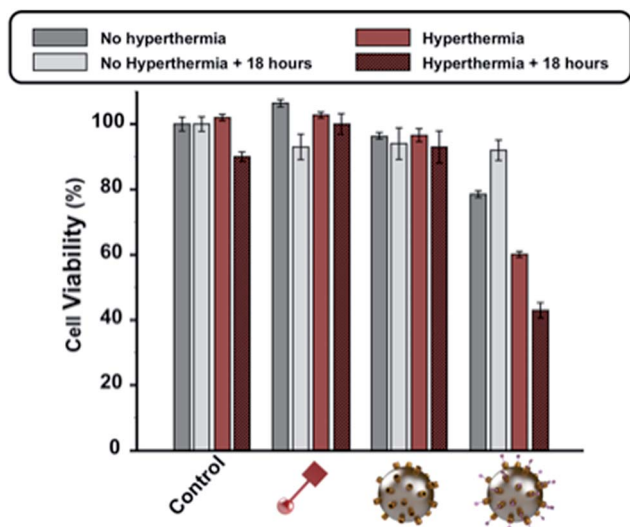
Fig. 6 HeLa cell viability in response to hyperthermia and chemotherapy. Cells were separated into four groups and incubated for two hours at 37 °C with growth medium alone (control), free Dox ([Dox] = 10 μM; red symbol with square), CB[7]NPs (sphere with yellow studs) or Dox@CB[7]NPs ([Dox] = 10 μM, sphere with yellow and purple studs). A sample from each treatment group was then subjected to an AMF (464 kHz) for one hour to induce hyperthermia. The viability of unheated samples was measured immediately after incubation (dark gray) and 18 hours after incubation (light gray). The viability of heated samples was measured immediately after AMF removal (light red) and 18 hours after AMF removal (dark red). Error bars represent standard deviations of triplicate measurements.

but not subjected to an AMF initially decreased to 78% but recovered to 92% after 18 hours. In contrast, the viability of cells incubated with Dox@CB[7]NPs and then subjected to one hour of an AMF initially decreased to 60% but then decreased further to 43% after an additional 18 hours, demonstrating a pronounced and long-term effect of the combined treatments.

***In vivo* toxicity assessment using *C. elegans*.** To assess the effect of nanoparticles *in vivo* we used *C. elegans*, a well-established model system for toxicity studies.[38,39,63] This free-living, non-pathogenic worm is an ideal animal model due to its small size, transparent body, rapid lifecycle, and conservation of genetic and cellular processes with higher organisms. In this study, L1 or L4 stage *C. elegans* larvae were cultured on nematode growth medium in the presence of CB[7]NPs or Dox@CB[7]NPs mixed with *E. coli* (OP50) bacteria as food source. Nanoparticles formed brown aggregates in the *C. elegans* digestive tract, which were confirmed using Prussian Blue staining (Fig. S22A and B†). Furthermore, adults incubated with CB[7]NPs were attracted to a permanent magnet, demonstrating the presence of internalized magnetic nanoparticles (Fig. S22C†). The mean quantity of iron that was internalized per worm corresponded to approximately 4.0×10^8 NPs.

To evaluate potential toxic effects on different aspects of worm development we monitored adult and embryonic survival, larval growth, and reproduction. Exposure to CB[7]NPs with iron concentration as high as 9 mM (500 mg L^{-1}) did not significantly affect adult worm survival to day 13 in the presence of fresh food (Fig. S23†). Similarly, progression through

different larval stages (L1 to adults) was insensitive to all concentrations of CB[7]NPs or Dox@CB[7]NPs tested (Fig. S24†). Finally, we tested the effect of exposure to CB[7]NPs or Dox@CB[7]NPs on embryonic development and brood size. While exposure to nanoparticles from the L4 stage did not affect viability of the progeny (data not shown) or brood size at iron concentrations up to 1.8 mM (100 mg L^{-1}), a significant reduction in brood size (~20%) was observed at the highest concentration of CB[7]NPs, corresponding to [Fe] = 9 mM (500 mg L^{-1}), with or without coupled doxorubicin (Fig. S24B†). This reduction can be attributed to the nanoparticles alone, since Dox coupling had no additional effect; exposure to free Dox at the same concentration (13 μM or 7.68 mg L^{-1}) also had no effect on brood size.

In this study, we examined the *in vivo* effects of CB[7]NPs up to much higher iron concentrations than reported in other studies[38-40,64] and found that exposure to CB[7]NPs up to 1.8 mM (100 mg L^{-1}) had no noticeable effect on growth, survival, or brood size. These results indicate that iron nanoparticles are well tolerated by *C. elegans* and constitute a promising first step toward future biocompatibility studies of our drug delivery system in higher organisms.[38,65]

Conclusions

CB[7]NPs were used to adsorb, deliver and release the anti-cancer therapeutic doxorubicin. Intracellular delivery, with gradual (low pH, GSH) or fast and on-demand (heat) release of Dox, was demonstrated in HeLa cells *in vitro*. The treatment of HeLa cells with both Dox@CB[7]NPs and subsequent AMF-induced hyperthermia was significantly more effective at reducing cell viability than either Dox or Dox@CB[7]NP treatment alone. The cytotoxic effects of Dox@CB[7]NPs were specific to the four cancer-derived cell lines tested, as no significant toxicity was observed in non-cancer-derived cells, which internalized the particles with two orders of magnitude lower efficiency. We also showed that the *in vivo* animal model *C. elegans* shows no impairment of survival, growth or fertility upon treatment with nanoparticle concentrations of up to at least 100 mg L^{-1}.

In summary, we have found surface-attachment of CB[7] to IONPs to be a facile, efficient, and cost-effective strategy for the preparation of a doxorubicin drug delivery system. In future studies, we plan to target specific diseased tissue by modifying the particles with bioactive moieties. With further development, Dox@CB[7]NPs could serve as a hybrid anti-cancer therapeutic.

Experimental section

Loading of CB[7]NPs with Dox

CB[7]NPs ($n_{CB[7]} = 1.3 \times 10^{-4}$ mol) and doxorubicin·HCl, *i.e.* Dox (1.5×10^{-4} mol) were mixed in water ($V = 3$ mL, CB[7]/Dox, 1 : 1.1) and stirred for 24 hours at room temperature and pH = 7 to form inclusion complexes on the surface of NPs. Slow dialysis was used to remove excess Dox that was not interacting with the CB[7] macrocycles on the surface of the NPs. The brown precipitate, Dox@CB[7]NPs, that was collected after dialysis was

analyzed by FTIR, TGA and ζ-potential measurements to confirm and quantify the adsorption of Dox to the CB[7]NPs.

Cell culture

Cervical epithelial cancer (HeLa; ATCC no. CCL-2), breast cancer (MCF-7, ATCC no. HTB-22) and non-cancer (Human Embryonic Kidney 293, HEK; ATCC no. CRL-1573) cells were cultured in Dulbecco's Modified Eagle's medium (DMEM), 10% fetal bovine serum (FBS), 1% penicillin/streptomycin and 20 mL L-glutamine at 5% CO_2 and 37 °C. Ovarian cancer (A2780, ECACC 93112519) and doxorubicin-resistant ovarian cancer cells (A2780/AD, ECACC 93112517) were cultured in Roswell Park Memorial Institute (RPMI)-1640 medium, 10% fetal bovine serum (FBS), 1% penicillin/streptomycin and 20 mL L-glutamine at 5% CO_2 and 37 °C.

Acknowledgements

References

1 M. Guba, P. von Breitenbuch, M. Steinbauer, G. Koehl, S. Flegel, M. Hornung, C. J. Bruns, C. Zuelke, S. Farkas, M. Anthuber, K. W. Jauch and E. K. Geissler, *Nat. Med.*, 2002, **8**, 128.

2 R. Hoffman, D. H. Paper, J. Donaldson and H. Vogl, *Br. J. Cancer*, 1996, **73**, 1183.

3 A. E. Kayl and C. A. Meyers, *Curr. Opin. Obstet. Gynecol.*, 2006, **18**, 24.

4 D. Peer, J. M. Karp, S. Hong, O. C. Farokhzad, R. Margalit and R. Langer, *Nat. Nanotechnol.*, 2007, **2**, 751.

5 A. Schroeder, D. A. Heller, M. M. Winslow, J. E. Dahlman, G. W. Pratt, R. Langer, T. Jacks and D. G. Anderson, *Nat. Rev. Cancer*, 2012, **12**, 39.

6 Y. Bae, N. Nishiyama, S. Fukushima, H. Koyama, M. Yasuhiro and K. Kataoka, *Bioconjugate Chem.*, 2005, **16**, 122.

7 O. Veiseh, J. W. Gunn and M. Zhang, *Adv. Drug Delivery Rev.*, 2010, **62**, 284.

8 X.-H. Peng, X. Qian, H. Mao, A. Y. Wang, Z. Chen, S. Nie and D. M. Shin, *Int. J. Nanomed.*, 2008, **3**, 311.

9 L. Babes, B. Denizot, G. Tanguy, J. J. Le Jeune and P. Jallet, *J. Colloid Interface Sci.*, 1999, **212**, 474.

10 S. Laurent, S. Dutz, U. O. Hafeli and M. Mahmoudi, *Adv. Colloid Interface Sci.*, 2011, **166**, 8.

11 F. Benyettou, I. Milosevic, Y. Lalatonne, F. Warmont, R. Assah, J.-C. Olsen, M. Jouaid, L. Motte, C. Platas-Iglesias and A. Trabolsi, *J. Mater. Chem. B*, 2013, **1**, 5076.

12 X.-L. Qiu, X. Zhou, X.-Y. Jin, A.-D. Qi and Y.-W. Yang, *J. Mater. Chem. C*, 2015, **3**, 3517.

13 W. L. Mock, in *Supramolecular Chemistry II—Host Design and Molecular Recognition*, ed. E. Weber, Springer Berlin Heidelberg, Berlin, Heidelberg, 1995, p. 1.

14 H. J. Buschmann, L. Mutihac, K. Jansen and E. Schollmeyer, *J. Inclusion Phenom. Macrocyclic Chem.*, 2005, **53**, 281.

15 I. Bernal, U. Mukhopadhyay, A. V. Virovets, V. P. Fedin and W. Clegg, *Chem. Commun.*, 2005, 3791.

16 A. L. Ortega, S. Mena and J. M. Estrela, *Cancers*, 2011, **3**, 1285.

17 Q.-L. Li, Y. Sun, Y.-L. Sun, J. Wen, Y. Zhou, Q.-M. Bing, L. D. Isaacs, Y. Jin, H. Gao and Y.-W. Yang, *Chem. Mater.*, 2014, **26**, 6418.

18 C. Marquez, R. R. Hudgins and W. M. Nau, *J. Am. Chem. Soc.*, 2004, **126**, 5806.

19 I. F. Tannock and D. Rotin, *Cancer Res.*, 1989, **49**, 4373.

20 K. Engin, D. B. Leeper, J. R. Cater, A. J. Thistlethwaite, L. Tupchong and J. D. McFarlane, *Int. J. Hyperthermia*, 1995, **11**, 211.

21 L. E. Gerweck and K. Seetharaman, *Cancer Res.*, 1996, **56**, 1194.

22 M. L. Circu and T. Y. Aw, *Biochim. Biophys. Acta*, 2012, **1823**, 1767.

23 X. Wang, X. Cai, J. Hu, N. Shao, F. Wang, Q. Zhang, J. Xiao and Y. Cheng, *J. Am. Chem. Soc.*, 2013, **135**, 9805.

24 R. Cheng, F. Feng, F. Meng, C. Deng, J. Feijen and Z. Zhong, *J. Controlled Release*, 2011, **152**, 2.

25 B. Khorsand, G. Lapointe, C. Brett and J. K. Oh, *Biomacromolecules*, 2013, **14**, 2103.

26 S. Mura, J. Nicolas and P. Couvreur, *Nat. Mater.*, 2013, **12**, 991.

27 M. Kim, K. Ock, K. Cho, S.-W. Joo and S. Y. Lee, *Chem. Commun.*, 2012, **48**, 4205.

28 C. R. Thomas, D. P. Ferris, J. H. Lee, E. Choi, M. H. Cho, E. S. Kim, J. F. Stoddart, J. S. Shin, J. Cheon and J. I. Zink, *J. Am. Chem. Soc.*, 2010, **132**, 10623.

29 E. Amstad, J. Kohlbrecher, E. Müller, T. Schweizer, M. Textor and E. Reimhult, *Nano Lett.*, 2011, **11**, 1664.

30 S. F. Medeiros, A. M. Santos, H. Fessi and A. Elaissari, *Int. J. Pharm.*, 2011, **403**, 139.

31 L. K. Bogart, G. Pourroy, C. J. Murphy, V. Puntes, T. Pellegrino, D. Rosenblum, D. Peer and R. Levy, *ACS Nano*, 2014, **8**, 3107.

32 R. Ivkov, S. J. DeNardo, W. Daum, A. R. Foreman, R. C. Goldstein, V. S. Nemkov and G. L. DeNardo, *Clin. Cancer Res.*, 2005, **11**, 7093s.

33 P. Moroz, S. K. Jones and B. N. Gray, *Int. J. Hyperthermia*, 2002, **18**, 267.

34 M. Gonzales-Weimuller, M. Zeisberger and K. M. Krishnan, *J. Magn. Magn. Mater.*, 2009, **321**, 1947.

35 J. Luo, N. L. Solimini and S. J. Elledge, *Cell*, 2009, **136**, 823.

36 J. D. Chris, *Int. J. Hyperthermia*, 2005, **21**, 745.

37 K. J. Chen, E. Y. Chaung, S. P. Wey, K. J. Lin, F. Cheng, C. C. Lin, H. L. Liu, H. W. Tseng, C. P. Liu, M. C. Wei, C. M. Liu and H. W. Sung, *ACS Nano*, 2014, **8**, 5105.

38 L. Gonzalez-Moragas, S.-M. Yu, E. Carenza, A. Laromaine and A. Roig, *ACS Biomater. Sci. Eng.*, 2015, **1**, 1129.

39 L. Gonzalez-Moragas, A. Roig and A. Laromaine, *Adv. Colloid Interface Sci.*, 2015, **219**, 10.

40 G. I. Dawlatsina, R. T. Minullina and R. F. Fakhrullin, *Nanoscale*, 2013, **5**, 11761.

41 M. F. Charao, C. Souto, N. Brucker, A. Barth, D. S. Jornada, D. Fagundez, D. S. Avila, V. L. Eifler-Lima, S. S. Guterres, A. R. Pohlmann and S. C. Garcia, *Int. J. Nanomed.*, 2015, **10**, 5093.

42 R. T. Minullina, Y. N. Osin, D. G. Ishmuchametova and R. F. Fakhrullin, *Langmuir*, 2011, **27**, 7708.

43 A. Scharf, A. Piechulek and A. von Mikecz, *ACS Nano*, 2013, **7**, 10695.

44 A. Pluskota, E. Horzowski, O. Bossinger and A. von Mikecz, *PLoS One*, 2009, **4**, e6622.

45 S. F. Chin, M. Makha, C. L. Raston and M. Saunders, *Chem. Commun.*, 2007, 1948, DOI: 10.1039/b618596g.

46 M. M. Yallapu, S. F. Othman, E. T. Curtis, B. K. Gupta, M. Jaggi and S. C. Chauhan, *Biomaterials*, 2011, **32**, 1890.

47 S.-F. Lee, X.-M. Zhu, Y.-X. J. Wang, S.-H. Xuan, Q. You, W.-H. Chan, C.-H. Wong, F. Wang, J. C. Yu, C. H. K. Cheng and K. C.-F. Leung, *ACS Appl. Mater. Interfaces*, 2013, **5**, 1566.

48 C. R. Thomas, D. P. Ferris, J.-H. Lee, E. Choi, M. H. Cho, E. S. Kim, J. F. Stoddart, J.-S. Shin, J. Cheon and J. I. Zink, *J. Am. Chem. Soc.*, 2010, **132**, 10623.

49 A. Manciulea, A. Baker and J. R. Lead, *Chemosphere*, 2009, **76**, 1023.

50 H.-J. Buschmann, L. Mutihac, R.-C. Mutihac and E. Schollmeyer, *Thermochim. Acta*, 2005, **430**, 79.

51 Y. Lalatonne, L. Motte, J. Richardi and M. P. Pileni, *Phys. Rev. E: Stat., Nonlinear, Soft Matter Phys.*, 2005, **71**, 011404.

52 C. de Montferrand, Y. Lalatonne, D. Bonnin, N. Lievre, M. Lecouvey, P. Monod, V. Russier and L. Motte, *Small*, 2012, **8**, 1945.

53 N. C. Bigall, C. Wilhelm, M.-L. Beoutis, M. García-Hernandez, A. A. Khan, C. Giannini, A. Sánchez-Ferrer, R. Mezzenga, M. E. Materia, M. A. Garcia, F. Gazeau, A. M. Bittner, L. Manna and T. Pellegrino, *Chem. Mater.*, 2013, **25**, 1055.

54 F. Benyettou, E. Guenin, Y. Lalatonne and L. Motte, *Nanotechnology*, 2011, **22**, 055102.

55 F. Benyettou, K. Nchimi-Nono, M. Jouiad, Y. Lalatonne, I. Milosevic, L. Motte, J.-C. Olsen, N. I. Saleh and A. Trabolsi, *Chem.–Eur. J.*, 2015, **21**, 4607.

56 J. Huang, L. Bu, J. Xie, K. Chen, Z. Cheng, X. Li and X. Chen, *ACS Nano*, 2010, **4**, 7151.

57 F. Benyettou, J. A. Ocadiz Flores, F. Ravaux, R. Rezgui, M. Jouiad, S. I. Nehme, R. K. Parsapur, J.-C. Olsen, P. Selvam and A. Trabolsi, *Chem.–Eur. J.*, 2016, **22**, 17020.

58 F. Geinguenaud, I. Souissi, R. Fagard, L. Motte and Y. Lalatonne, *Nanomedicine*, 2012, **8**, 1106.

59 A. Yamagishi, *J. Magn. Magn. Mater.*, 1990, **90**, 43.

60 J. Huwyler, A. Cerletti, G. Fricker, A. N. Eberle and J. Drewe, *J. Drug Targeting*, 2002, **10**, 73.

61 A. Gabizon, H. Shmeeda and Y. Barenholz, *Clin. Pharmacokinet.*, 2003, **42**, 419.

62 D. Li, Y.-T. Zhang, M. Yu, J. Guo, D. Chaudhary and C.-C. Wang, *Biomaterials*, 2013, **34**, 7913.

63 M. C. Leung, P. L. Williams, A. Benedetto, C. Au, K. J. Helmcke, M. Aschner and J. N. Meyer, *Toxicol. Sci.*, 2008, **106**, 5.

64 Q. Wu, Y. Li, M. Tang and D. Wang, *PLoS One*, 2012, **7**, e43729.

65 P. H. Harlow, S. J. Perry, S. Widdison, S. Daniels, E. Bondo, C. Lamberth, R. A. Currie and A. J. Flemming, *Sci. Rep.*, 2016, **6**, 22965.